SUPPLEMENTAL MATERIAL

SUPPLEMENTAL MATERIALS AND METHODS

Kymograph analysis

In contrast to nanometer-scale tracking of bright fluorescent molecules using 2D Gaussian fitting algorithms, kymographs offer a quick and easy way to extract information about motor velocity and processivity without needing to localize dye molecules with sub-pixel precision. Generally, kymographs of fluorescence-tagged microtubule (MT) motors are made using a single, hand-drawn path along the MT long axis. For each image in the acquired time series, the intensity profile is calculated along this path, with each profile composing a single column of pixels along the spatial axis of the output image. Repeating this process for all frames yields the equivalent of a graph that plots the motor trajectory, i.e. position vs. time or as commonly done, time vs. position (Fig. 6A, main text).

Unfortunately, in practice, it is tedious and difficult to draw a single-pixel path such that the maximum intensity of every fluorescent spot always falls along the selected pixels (e.g. due to fluctuations in motor position along the direction orthogonal to the MT, long-term stage drift, small imprecisions in drawing of the line, etc.). As a result, even if the fluorescence intensity were absolutely constant, the intensity of the path traced-out in the kymograph can vary considerably, giving the false impression that the dye intensity fluctuates in time (in reality, the fluorescence intensity does fluctuate, due to the inherent photophysics, and the artificial fluctuations are added to this behavior). In other words, because the kymograph does not integrate the spot intensity over space, but rather shows a single line profile through an arbitrary point on the spot, information about the spot brightness is discarded, and artificial noise is introduced. This degrades the quality of the kymograph image, and also precludes quantitative analysis of the path intensities.

We solved this problem by creating a composite kymograph from several individual kymographs that are derived from paths parallel to the original one. First, as in a traditional kymograph, a path is drawn along the MT axis, and a kymograph is constructed from this line and saved. Next, the path is displaced by ±0.5 pixels perpendicular to the original path (so the paths are all parallel) and kymographs are again created from these paths and saved (intensities are calculated using the MATLAB 'improfile()' function, which interpolates inter-pixel values along line segments). The process is repeated four times, yielding a total of nine kymographs. While the intensities of the motor trajectories traced out in each of these kymographs varies, the trajectories themselves essentially overlap. These images are averaged together to create the final composite kymograph. This strategy makes use of the fact that the intensity missed by any individual kymograph will be detected by others derived from the parallel paths (i.e. it is an approximate integration over the intensity of the fluorescent spots). Consequently, variations in intensity of the paths in the composite kymograph are attributable to true variations in emitted fluorescence. This allows us to reliably quantify the number of fluorophores attached to each moving particle.

To analyze the fluorescence intensities using the improved kymograph, we identify the maximum intensity for each trajectory at each point in time. The trajectories are identified manually by drawing a path through the approximate center of each one. For each point in time, i.e. column of pixels in the kymograph, a search is conducted in 0.5 pixel increments above and below the point marked by the manually drawn path, and the maximum value is recorded. This technique precludes erroneous measurement of intensity fluctuations that would otherwise arise due to variations in motor velocity on short time scales, if only the approximate, manually drawn path were considered. For each path, plotting a histogram of intensities allows rapid, precise comparison of intensities between different particles (by comparing mean intensities), and determination of photobleaching over time (multi-modal distributions).

The methods described above allow rapid determination of motor velocity, run length, and stoichiometry without the computational demands of single-particle tracking. We have written user-friendly software to help perform this analysis, which we will describe in detail in a future publication.

SUPPLEMENTAL FIGURES

FIGURE S1. Hydrogen-bonding network matrix comparing the interactions between Dyn2 and Pac11 pep2 (upper horizontal axis) determined in this study with the previously reported interactions between Dyn2 and Nup159 pep2 (lower horizontal axis)(Romes *et al.*, 2012). Secondary structure is indicated along the axes as are residues involved in the interactions and their respective chain label. The top half of a grid square represents hydrogen bonds between Dyn2 and Pac11 pep2 while the bottom half represents hydrogen bonds between Dyn2 and Nup159 pep2. Backbone/backbone, side chain/side chain and backbone/side chain hydrogen bonds are colored blue, green, and red respectively. The number of hydrogen bonds that occur between two residues is one unless otherwise noted in by a "2" in the cell, indicative of two hydrogen bonds occurring between these residues. Where two of the designated hydrogen bonding classes occur between residues, the cell is split diagonally with each half colored accordingly.

FIGURE S2. Dyn2 is a homodimer in solution. SEC-MALS of WT Dyn2 was performed by injecting 50 µL of 6 mg/mL Dyn2 at pH 6.8. The differential refractive index was normalized to the dimer peak (21.6 kDa) and is shown in grey. Peaks from the differential refractive index display the measured molecular weight (black trace) with the corresponding fraction of total injected mass in parentheses. The WT Dyn2 construct has a calculated molecular weight of 10.9 kDa.

FIGURE S3. Dyn2 mutations at the Pac11 pep2 binding site as well as the Dyn2 homodimerization interface abrogate the ability of Dyn2 to bind Pac11 pep2 as detected using ITC. **A**. The upper panel shows heat generated by 19 x 2 µL sequential injections of 0.5 mM Pac11 pep2 (desalted using a G-25 Sephadex column, see Materials and Methods section), injected into the ITC cell containing 200 µL of 50 µM Dyn2 F76K/Y78E. The bottom panel shows normalized heat (Kcal/Mole of injectant) versus the molar ratio of Pac11 pep2:Dyn2 F76K/Y78E. No binding was detected. **B**. A control experiment in which an elevated concentration of Pac11 pep2 (3mM) obtained without desalting, was injected into the ITC cell containing 200 µL of sample buffer using the same injection protocol as in A. Exothermic heat of dilution was detected. **C**. Same as in B except the ITC cell contained 200 µL of 0.3 mM Dyn2 F76K/Y78E. The bottom panel shows normalized heat (Kcal/Mole of injectant) versus the molar ratio of Pac11 pep2:Dyn2 F76K/Y78E after subtracting the heat of dilution of Pac11 pep2 obtained in B. No binding was detected. **D**. Same as in A except the injectant was 0.5 mM Pac11 pep2 (desalted) and the ITC cell contained 200 µL of 50 µM Dyn2 H58K. No binding was detected. **E**. Same as in A except the injectant was 3 mM Pac11 pep2 (not desalted), and the ITC cell contained 200 µL of 0.3 mM Dyn2 H58K. No binding was detected.

FIGURE S4. TIRF-based, single-molecule fluorescence analysis confirms that the majority of TMR-labeled Dyn1 molecules purified from the WT strain is bound to Pac11-Myc, as revealed by the ~60% co-localization (yellow) of TMR-labeled Dyn1 (red) and Cy5-labeled anti-Myc antibodies (green) (top). In contrast, Dyn1 motors purified from the *dyn2*Δ (center) and *dyn2*Δ*pac11*Δ strains (bottom) do not show significant TMR-Cy5

co-localization (see supplemental material for details underlying this analysis). Images represent 330 × 330 pixel subregions of the original 512 × 512 pixel EMCCD images.

FIGURE S5. The absence of Dyn2/Pac11 results in an increased number of fluorescent spots bound to the coverslip surface that contain more than two dyes, suggesting Dyn1 aggregation. **A.-C.** Images show Cy5-labeled microtubules (green) and TMR-labeled Dyn1 (red) purified from WT (A), *dyn2*Δ (B) and *dyn2*Δ*pac11*Δ (C) strains, respectively (see Materials and Methods for details) (images represent 130 × 130 pixel subregions of the original 512 × 512 pixel EMCCD images). White arrows in B and C show examples of bright fluorescent spots containing more than two dyes. The white square in B indicates the subregion shown in D. **D.** A putative dynein aggregate containing more than three dyes, as revealed by intensity analysis (F). **E.** Kymograph generated by stacking line scans along the dashed line indicated in subfigure D (averaged with two parallel scans on each side, each separated by 0.5 pixels (effective pixel size: 160 nm); note that the smaller spot to the upper left of the aggregate marked "2." is a separate spot, not included in the line scans or other analysis). The kymograph shows the binding of two different-sized dynein complexes (steps 1. and 2.), followed by the bleaching/dissociation of one of the dyes/labeled Dyn1 HC attached to the first complex. The time marked t_1 corresponds to the image shown in B. **F.** Intensity analysis of the kymograph reveals that the first complex contains two dyes initially ($2 \times \Delta I \simeq 1.3$ a.u.), while the second complex contains more than four ($>4 \times \Delta I$). After the bleaching of one TMR molecule, the remaining fluorescence of the first complex reflects the intensity of a single dye ($\Delta I \simeq 1.3$ a.u. above background).

FIGURE S6. Fluorescence time traces and photobleaching analysis of TMR-tagged Dyn1. **A.** Example traces of fluorescence signals showing i) binding of a Dyn1 molecule to the coverslip surface, followed by the stepwise bleaching of both dyes (red), ii) 1-step bleaching of a single dye (green) of a Dyn1 molecule bound to the coverslip (dimer or monomer), and iii) the surface binding of a Dyn1 molecule with one dye (blue) (see Material and Methods for details). Intensities at each time point correspond to the average intensities in a square of 5x5 pixels with the pixel registering the highest relative counts centered on the 5 x 5 grid as calculated by ImageJ (NIH) (note that the intensity values calculated here cannot be directly compared to the intensities values presented in the kymograph-based analysis, which were calculated in a different way, see Supplemental Materials and Methods, Kymograph analysis). **B.** Photobleaching of TMR-tagged Dyn1 molecules covalently bound to a BSA-coated coverslip acquired under the same biochemical (dynein motility buffer plus additives, see Materials and Methods) and photophysical conditions (fluorescence excitation intensity) as used for the single-molecule assay except that images were captured once per second. Intensities at each time point correspond to the total intensities in each acquired image. Fitting a first-order exponential decay function yields a characteristic time before bleaching of 271 ± 2 s, which corresponds to an average photobleaching rate of 0.0037 s^{-1}.

SUPPLEMENTAL REFERENCES

Kardon, J.R., Reck-Peterson, S.L., and Vale, R.D. (2009). Regulation of the processivity and intracellular localization of Saccharomyces cerevisiae dynein by dynactin. Proc Natl Acad Sci U S A *106*, 5669-5674.

Romes, E.M., Tripathy, A., and Slep, K.C. (2012). Structure of a yeast Dyn2-Nup159 complex and molecular basis for dynein light chain-nuclear pore interaction. J Biol Chem *287*, 15862-15873.

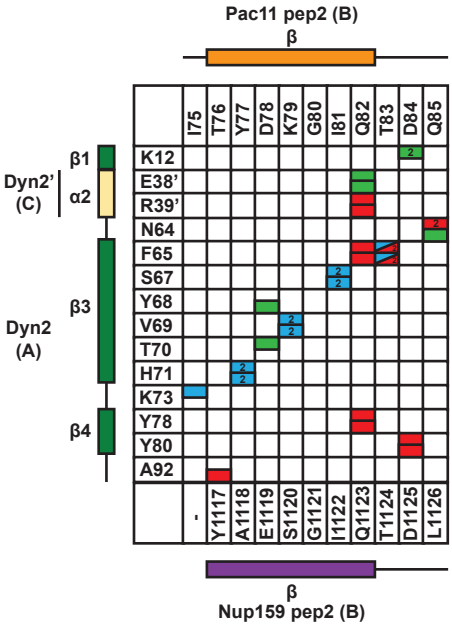
Pac11 pep2 (B)
β
I75
T76
Y77
D78
K79
G80
I81
Q82
T83
D84
Q85
β1
Dyn2'
(C)
α2
K12
E38'
R39'
N64
F65
S67
β3
Dyn2
(A)
Y68
V69
T70
H71
K73
β4
Y78
Y80
A92
-
Y1117
A1118
E1119
S1120
G1121
I1122
Q1123
T1124
D1125
L1126
β
Nup159 pep2 (B)

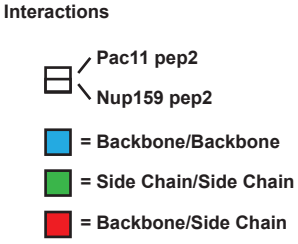
Interactions
Pac11 pep2
Nup159 pep2
= Backbone/Backbone
= Side Chain/Side Chain
= Backbone/Side Chain

Fig. S1

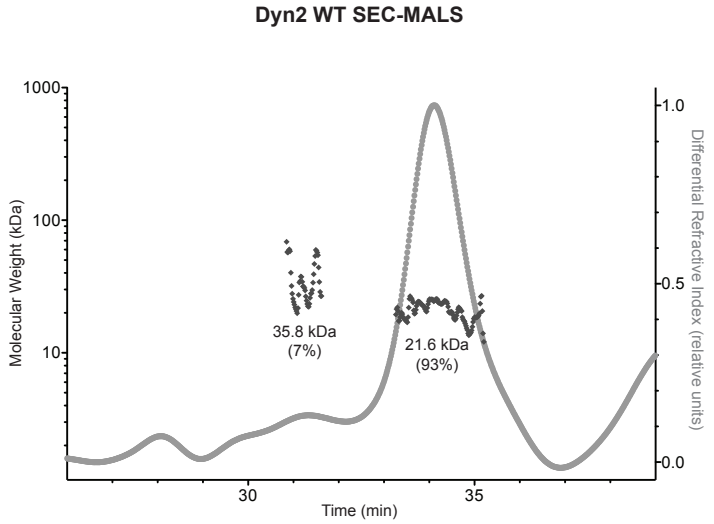
Dyn2 WT SEC-MALS
1000
100
10
Molecular Weight (kDa)
1.0
0.5
0.0
Differential Refractive Index (relative units)
35.8 kDa
(7%)
21.6 kDa
(93%)
30
35
Time (min)

Fig. S2

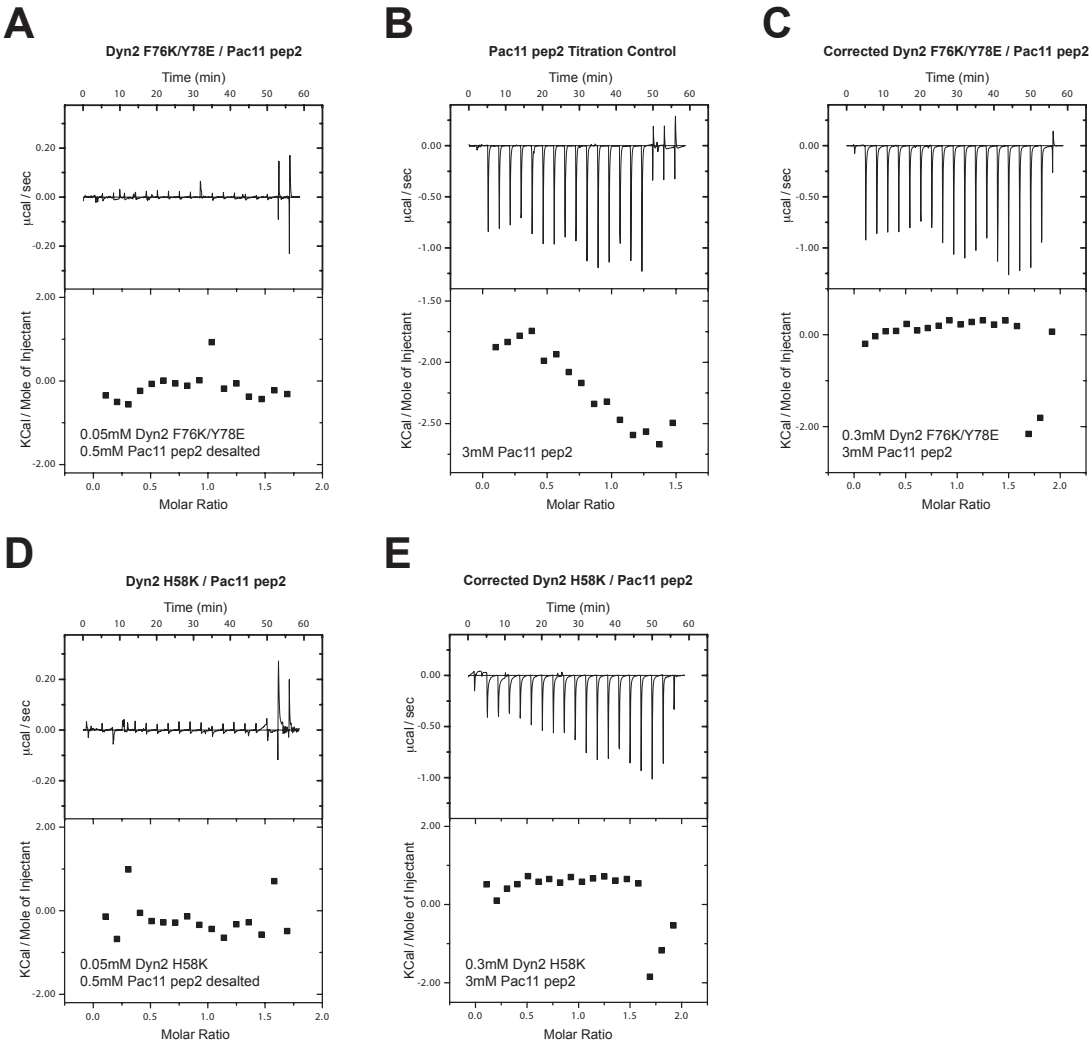
A
Dyn2 F76K/Y78E / Pac11 pep2
Time (min)
µcal / sec
KCal / Mole of Injectant
0.05mM Dyn2 F76K/Y78E
0.5mM Pac11 pep2 desalted
Molar Ratio
B
Pac11 pep2 Titration Control
Time (min)
µcal / sec
KCal / Mole of Injectant
3mM Pac11 pep2
Molar Ratio
C
Corrected Dyn2 F76K/Y78E / Pac11 pep2
Time (min)
µcal / sec
KCal / Mole of Injectant
0.3mM Dyn2 F76K/Y78E
3mM Pac11 pep2
Molar Ratio
D
Dyn2 H58K / Pac11 pep2
Time (min)
µcal / sec
KCal / Mole of Injectant
0.05mM Dyn2 H58K
0.5mM Pac11 pep2 desalted
Molar Ratio
E
Corrected Dyn2 H58K / Pac11 pep2
Time (min)
µcal / sec
KCal / Mole of Injectant
0.3mM Dyn2 H58K
3mM Pac11 pep2
Molar Ratio

Fig. S3

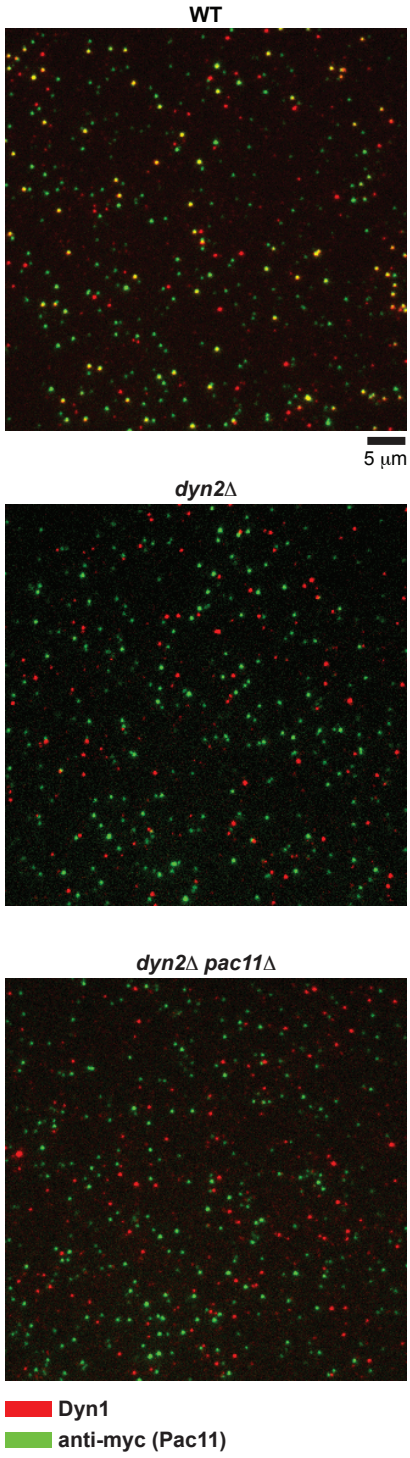

Fig. S4

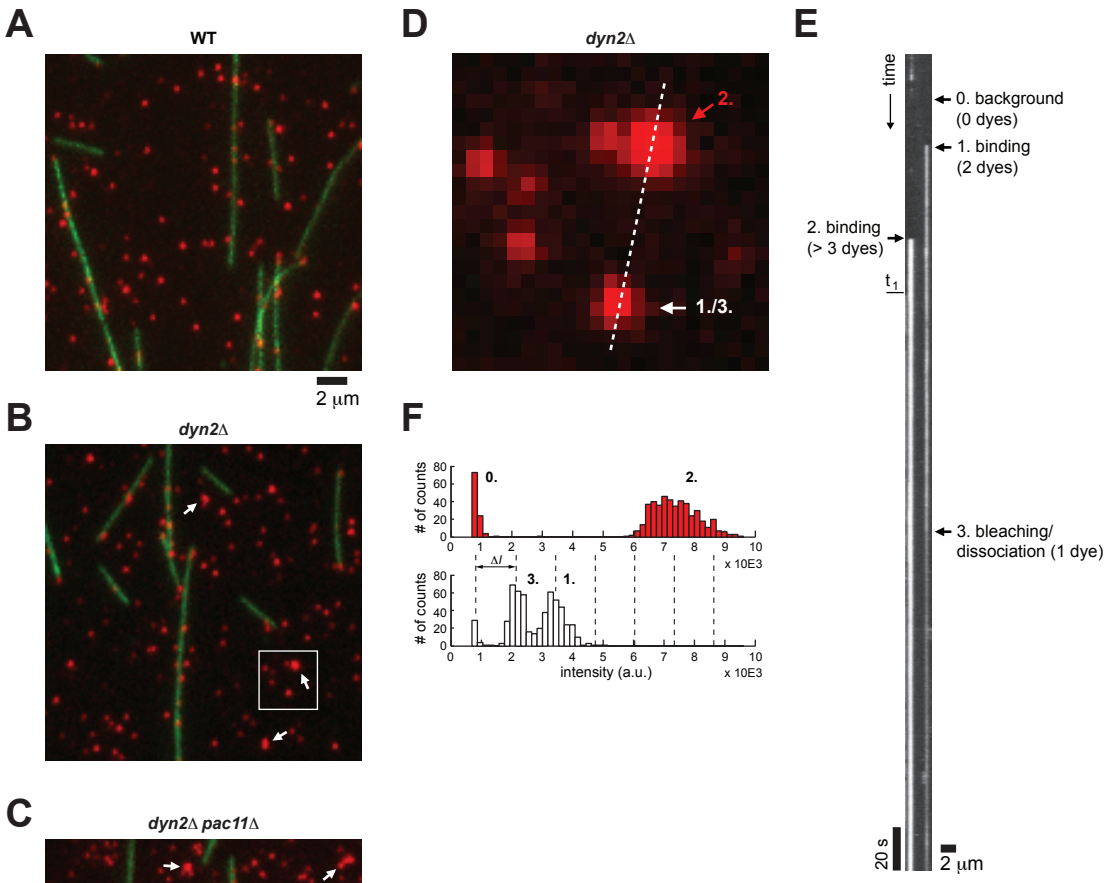
A
WT
2 μm
B
dyn2Δ
C
dyn2Δ pac11Δ
D
dyn2Δ
2.
1./3.
E
time
0. background
(0 dyes)
1. binding
(2 dyes)
2. binding
(> 3 dyes)
t1
3. bleaching/
dissociation (1 dye)
20 s
2 μm
F
# of counts
0.
2.
x 10E3
Δl
3.
1.
intensity (a.u.)

Fig. S5

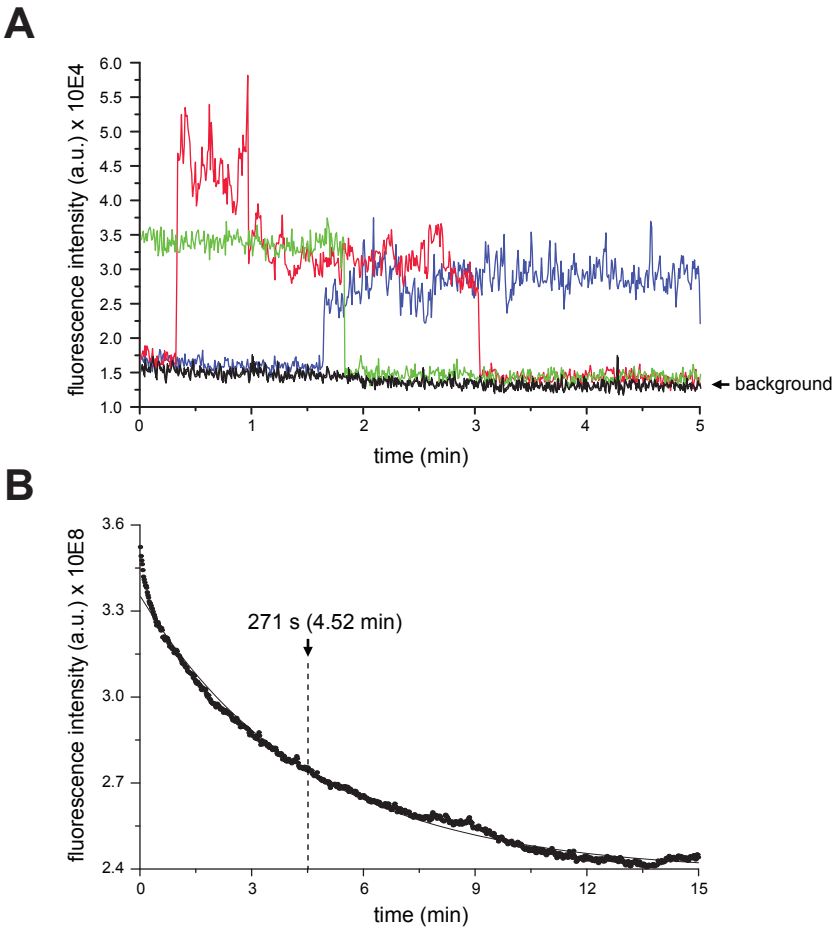
A
fluorescence intensity (a.u.) x 10E4
6.0
5.5
5.0
4.5
4.0
3.5
3.0
2.5
2.0
1.5
1.0
0
1
2
3
4
5
time (min)
background
B
fluorescence intensity (a.u.) x 10E8
3.6
3.3
3.0
2.7
2.4
271 s (4.52 min)
0
3
6
9
12
15
time (min)

Fig. S6

TABLE S1: Yeast strain genotype.

Strain	Note	Genotype	Source
VY263		pep4::HIS3, prb1Δ, PAC11-13×Myc::TRP, ZZ-TEV-GFP-3×HA-DYN1-GS-HALOTAG::KAN, nip100Δ::URA3	Kardon *et al.*, 2009.
GY4	VY263 with *dyn2Δ*	pep4::HIS3, prb1Δ, PAC11-13×Myc::TRP, ZZ-TEV-GFP-3×HA-DYN1-GS-HALOTAG::KAN, nip100Δ::URA3, dyn2Δ::NAT	this study
GY6	VY263 with *dyn2Δ* and *pac11Δ*	pep4::HIS3, prb1Δ, ZZ-TEV-GFP-3×HA-DYN1-GS-HALOTAG::KAN, nip100Δ::URA3, dyn2Δ::NAT, pac11Δ::HYG	this study

TABLE S2: Quantification of dye-labels in mobile versus immobile Dyn1 populations.

Strain	Mobile	1 dye mobile	2 dye mobile	≥3 dye mobile	1 dye immobile	2 dye immobile	≥3 dye immobile
VY263 % (n)	60.5±2.2 (885)	34.3±2.8 (535)	64.4±2.9 (535)	1.3 (535)	57.7±4.0 (350)	38.7±3.8 (350)	3.6 (350)
GY4 % (n)	21.5±1.4 (867)	30.6±4.1 (186)	68.3±4.2 (186)	1.1 (186)	81.1±1.8 (681)	17.5±1.8 (681)	1.4 (681)
GY6 % (n)	22.3±1.4 (1238)	38.1±3.9 (276)	61.6±4.0 (276)	0.3 (276)	79.9±1.8 (962)	18.5±1.7 (962)	1.6 (962)